Flexible Voltage Support Control for Three-Phase Distributed Generation Inverters Under Grid Fault

Antonio Camacho, Miguel Castilla, Jaume Miret, *Member, IEEE*, Juan C. Vasquez, and Eduardo Alarcón-Gallo

***Abstract*—Ancillary services for distributed generation (DG) systems become a challenging issue to smartly integrate renewable-energy sources into the grid. Voltage control is one of these ancillary services which can ride through and support the voltage under grid faults. Grid codes from the transmission system operators describe the behavior of the energy source, regulating voltage limits and reactive power injection to remain connected and support the grid under fault. On the basis that different kinds of voltage sags require different voltage support strategies, a flexible control scheme for three-phase grid-connected inverters is proposed. In three-phase balanced voltage sags, the inverter should inject reactive power in order to raise the voltage in all phases. In one- or two-phase faults, the main concern of the DG inverter is to equalize voltages by reducing the negative symmetric sequence and clear the phase jump. Due to system limitations, a balance between these two extreme policies is mandatory. Thus, over- and undervoltage can be avoided, and the proposed control scheme prevents disconnection while achieving the desired voltage support service. The main contribution of this work is the introduction of a control algorithm for reference current generation that provides flexible voltage support under grid faults. Two different voltage sags have been experimentally tested to illustrate the behavior of the proposed voltage support control scheme.**

***Index Terms*—Reactive power control, voltage ride through, voltage sag, voltage support.**

I. Introduction

TOTAL installed power from renewable-energy sources is constantly growing in the new electric deregulated scenario. Among them, photovoltaic and wind turbine are gaining increasing attention in the last few years [1], [2]. When connected to the grid, renewable-energy sources behave as distributed generation (DG) systems. The inclusion of DG systems is changing the paradigm of energy production [3]. Microgrids and smart energy networks [4]–[7] are receiving increased interest because of their potential advantages over conventional centralized systems; one of these advantages is that the energy production takes place closer to the consumer and, thus, real and reactive power losses can be minimized [8]. The inclusion of ancillary services allows for better resource utilization of the transmission system. Although, currently, new requirements are mainly focused on wind farms, in a near future, these requirements could be extended to small distributed suppliers [9].

The basic element for interconnecting DG to the transmission system is the three-phase inverter. In normal grid conditions, three-phase DG inverters inject all the generated active power into the grid. One of the major drawbacks for proper operation of the whole system occurs when a voltage sag (dip) is transmitted through the network. In grid fault conditions, the controller must react to the perturbation and mitigate the adverse effects on the inverter side. Depending on the depth and duration of the voltage sag, the grid codes force disconnection of the system. Under current regulations, grid codes, available from transmission system operators (TSOs), dictate the behavior of the customer under voltage sags [10]–[12]. However, in grids with high penetration of renewable-energy sources, conventional regulations are under revision. In addition, these codes do not take into account the shape of the voltage fault but only the root mean square (rms) voltage. In this paper, a flexible control algorithm is proposed to face the problem of different types of voltage sags. Whenever balanced three-phase voltage sags occur, the voltage support strategy should raise the voltage in all phases as much as possible. However, if only one or two phases are in fault, a voltage equalizing strategy will be of interest. Voltage equalization is accomplished when the difference between rms voltages is reduced. Then, it is possible to avoid undervoltage in the phases under fault or overvoltage in the phases that do not suffer the voltage sag. Moreover, the negative-sequence voltage is reduced and the phase jump is cleared, which are important arguments to properly operate DG inverters [13]. To avoid disconnection, phase voltages must remain within upper and lower limits. Thus, a flexible strategy combining raising and equalizing capabilities, as proposed here, could be a better solution than conventional voltage support strategies to prevent from disconnection by under-/overvoltage.

Novel control schemes are needed for a greater penetration of DG sources. Better control algorithms improve power quality and efficiency and increase grid reliability as well [14]. Therefore, control schemes with higher performance are the basis for proper operation of DG systems, particularly under grid faults. Many control algorithms designed to deal with grid disturbances are based on symmetric components [15]–[23]. Among them, the contribution of [17] deserves special attention for selecting active power quality characteristics; further research was done in [18] for reactive power. Based on symmetric

Manuscript received April 29, 2011; revised October 14, 2011 and December 20, 2011; accepted December 30, 2011. Date of publication January 18, 2012; date of current version November 22, 2012. This work was supported by the Spanish Ministry of Science and Technology under Grant ENE2009-13998-C02-01.

A. Camacho, M. Castilla, J. Miret, and E. Alarcón-Gallo are with the Department of Electronic Engineering, Technical University of Catalonia, 08800 Vilanova i la Geltrú, Spain (e-mail: antonio.camacho.santiago@upc.edu; miquel.castilla@upc.edu; jmiret@eel.upc.edu; eduardo.alarcon-gallo@upc.edu)

J. C. Vasquez is with the Department of Energy Technology, Aalborg University, 9220 Aalborg, Denmark (e-mail: juq@et.aau.dk)

Digital Object Identifier 10.1109/TIE.2012.2185016

components, Alepuz *et al.* [19] and Etxeberria-Otadui *et al.* [20] analyze active and reactive power oscillations. In [20], three control strategies under unbalanced grid voltages are compared in order to achieve optimal power quality characteristics focused on dc-link voltage optimization, power exchange maximization, and a combination of the two. An interesting work was proposed in [21] to get smooth active power characteristics by grouping some of the strategies presented in [17]. In [22], the work in [21] is analyzed for both active and reactive powers. In [23], an extended generalization of [21] and [17] is formulated to achieve particular power characteristics such as total harmonic distortion and power oscillations. However, none of the previously mentioned works take care of the voltage sag shape (i.e., either three-phase, unbalanced single-phase, or unbalanced two-phase fault), given that the control strategies are not specifically designed to better ride through different kinds of voltage sags.

This paper is organized as follows. Section II formulates the problem. Section III analyzes conventional control schemes under grid faults and proposes the new voltage support control scheme. Section IV analyzes power quality characteristics. Section V presents numerical examples of the theoretical power quality characteristics. Section VI shows two selected experimental tests to validate the proposed algorithm. Section VII concludes this paper.

II. Problem Formulation

This paper focuses on current-mode three-phase inverters to smartly support the grid voltage under fault. Inverter behavior is commanded by the controller unit, which, according to [24] and [25], has to fulfill the following requirements:

1) active power control;
2) reactive power control;
3) voltage ride through;
4) reactive current injection;
5) high power quality.

In normal grid conditions, DG inverters must regulate both active and reactive powers injected into the grid. When the grid is in fault, voltage support control can mitigate voltage sag effects by injecting additional reactive current to ride through the perturbation and support the grid voltage. High quality of the injected currents is obtained when no harmonic distortion is present in the grid currents even during grid faults.

A. Three-Phase DG Inverter

Fig. 1 shows the typical configuration of a three-phase DG inverter. The complete system is composed of the power source (PS), the inverter, and the grid. Interconnection between the PS and the inverter is operated by a dc-link capacitor. The control of the dc-link voltage v_{dc} balances the power flow in the system. The inverter consists of a three-leg voltage-source pulsewidth-modulation inverter with an LCL filter to reduce high-frequency harmonics [26]. To avoid filter resonance, a passive damping resistor is included in series with the capacitor [27]. Finally, the DG inverter is connected to the grid at the point of common coupling (PCC). Grid impedance is mainly

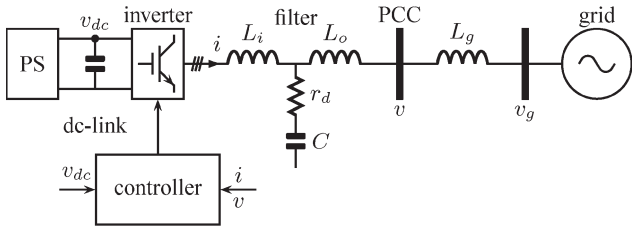

Fig. 1. Grid-connected three-phase DG inverter.

inductive, so the inductance L_g is used to model the connection between the three-phase DG inverter and the grid. Grid voltage v_g can be affected by the fault produced somewhere in the transmission system.

B. Voltage Sag Characterization

A voltage sag is an abnormal condition in the grid voltages, characterized by a short-time reduction in one or various phases [28]. The causes of voltage sags are mainly phase-to-ground short circuit, phase-to-phase (to ground) short circuit, and the start-up of large motors [29]. The most widely accepted classification of voltage sags is presented in [30].

Voltage sags can be characterized by the module, frequency, and initial angle of each phase or by the positive, negative, and zero symmetric sequences

$$v_a = v_a^+ + v_a^- + v_a^0 \tag{1}$$
$$v_b = v_b^+ + v_b^- + v_b^0 \tag{2}$$
$$v_c = v_c^+ + v_c^- + v_c^0 \tag{3}$$

where the super indexes (+, −, and 0) indicate the positive, negative, and zero symmetric sequences, respectively. In three-wire systems, zero sequence voltage v^0 and current i^0 are not present [31].

Instead of using a natural frame for characterizing the grid voltage, the Clarke transformation is applied to express measured voltages in the stationary reference frame (SRF)

$$\begin{bmatrix} v_\alpha \\ v_\beta \end{bmatrix} = \frac{1}{3}\begin{bmatrix} 2 & -1 & -1 \\ 0 & \sqrt{3} & -\sqrt{3} \end{bmatrix}\begin{bmatrix} v_a \\ v_b \\ v_c \end{bmatrix}. \tag{4}$$

Using this transformation in three-wire systems, (1)–(3) can be expressed as

$$v_\alpha = v_\alpha^+ + v_\alpha^- \tag{5}$$
$$v_\beta = v_\beta^+ + v_\beta^- \tag{6}$$

where v_α^+ and v_β^+ are the positive-sequence voltages in the SRF and v_α^- and v_β^- are the negative ones.

Positive and negative voltage sequences as functions of time can be represented as

$$v_\alpha^+ = V^+ \cos(\omega t + \varphi^+) \tag{7}$$
$$v_\beta^+ = V^+ \sin(\omega t + \varphi^+) \tag{8}$$
$$v_\alpha^- = V^- \cos(\omega t - \varphi^-) \tag{9}$$
$$v_\beta^- = -V^- \sin(\omega t - \varphi^-) \tag{10}$$

where V^+ and V^- are the amplitudes of the positive and negative sequences, respectively, ω is the grid frequency, and φ^+ and φ^- are the initial phase angles of positive and negative sequences, respectively. It should be noted that V^+, V^-, ω, φ^+, and φ^- can be time-varying parameters. However, for the sake of simplicity, in this work, they are assumed constant during the sag.

A useful parameter to characterize the voltage sag is the voltage unbalance factor (n) [13]. This parameter describes the amount of imbalance in the system as the ratio between negative and positive voltage amplitudes

$$n = \frac{V^-}{V^+} = \frac{\sqrt{\left(v_\alpha^-\right)^2 + \left(v_\beta^-\right)^2}}{\sqrt{\left(v_\alpha^+\right)^2 + \left(v_\beta^+\right)^2}}. \tag{11}$$

Some standards [32], [28] recommend $n < 0.02$ in normal operation to avoid malfunctioning problems due to imbalances.

C. Grid Code Requirements

TSO requirements in grid codes state that power generators should remain connected even in faulted grid conditions in order to feed the grid and support the grid voltage. Different TSOs provide different voltage profiles as limits for disconnection [11], [24], depending on sag depth and duration. During a short interval (typically, less than 0.150 s), the inverter must remain connected even in very deep sag conditions [0.2 per unit (p.u.)]. In moderate voltage sags (below 0.8 p.u.), the inverter must remain connected for a longer time (2 s).

Another issue in voltage support requirements is the reactive/active power ratio. In deep voltage sags, only the reactive power must be injected to the grid. However, in less deep voltage sags, both active and reactive powers must be transferred to keep feeding the grid [24], [33].

D. Control of Three-Phase DG Inverter Under Fault

The behavior of the current-mode three-phase inverter is determined by the injected current at the PCC. By injecting reactive power into the grid, the rms voltage at the PCC can be increased to support the grid voltage under fault. Then, a proper reference current generator is required when the grid is under fault in order to counteract the voltage sag effects on the system. In Fig. 2, a block diagram of the controller for DG inverters under grid fault is shown.

The inputs of the controller are the measured phase voltages v at the PCC, the currents i flowing through L_i inductor [27], and the dc-link voltage v_{dc}. Voltage v and current i are transformed into SRF values. Voltages v_α and v_β are then decomposed into symmetric components using a sequence extractor. The symmetric sequence extractor is a key aspect to characterize the grid voltage. Many sequence extractors can be found in the literature to extract voltage sag information at run time [34]–[38]. The dc-link voltage regulator is in charge of the active power reference P^* that keeps power balance.

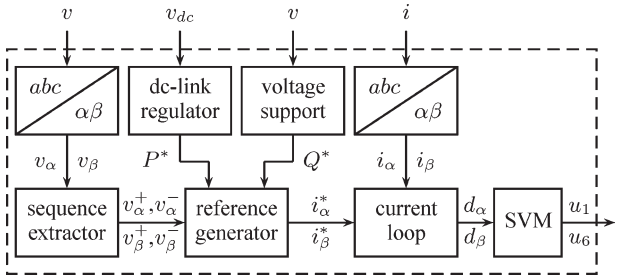

Fig. 2. Control diagram of three-phase DG inverter under grid fault.

The voltage support block needs first to detect the voltage sag. This can be done by computing the voltage rms in each phase. When one or several rms values drop below a predefined threshold, the voltage support control is activated. The voltage support block decides which strategy should be implemented according to grid codes and system limitations. This part provides the reactive power reference Q^*; for the sake of simplicity, in this study, this reference is computed offline, and no closed loop is implemented. All this information passes through the reference generator to build reference currents i_α^* and i_β^*. The reference current generator is the kernel of the control algorithm because it can flexibly support the grid voltage. The next stage corresponds to the current loop, where the references are compared with the measured currents. At the end of the current control loop, duty cycles d_α and d_β are processed by the space vector pulsewidth modulator to commute the switches $u_1, u_2, \ldots, u_6$.

The main objective of this work is to present a method to ride through voltage sags and support the grid voltage. In three-phase balanced voltage sags, the control strategy should be to raise the voltage in all phases. In one- or two-phase voltage sags, the controller is in charge of a grid current that equalizes voltages, i.e., keeps peak values within acceptable limits.

III. From Conventional to Proposed Control

Under balanced grid conditions, the inverter extracts the maximum active power from the source and injects it into the grid. In this ideal scenario, the reference currents for active power can be expressed as [39]

$$i_{\alpha(p)}^* = \frac{2}{3} P^* \frac{v_\alpha}{(v_\alpha)^2 + (v_\beta)^2} \tag{12}$$

$$i_{\beta(p)}^* = \frac{2}{3} P^* \frac{v_\beta}{(v_\alpha)^2 + (v_\beta)^2} \tag{13}$$

where P^* is the active power reference from the dc-link voltage loop.

Similar equations can be applied to reactive power injection

$$i_{\alpha(q)}^* = \frac{2}{3} Q^* \frac{v_\beta}{(v_\alpha)^2 + (v_\beta)^2} \tag{14}$$

$$i_{\beta(q)}^* = \frac{2}{3} Q^* \frac{-v_\alpha}{(v_\alpha)^2 + (v_\beta)^2} \tag{15}$$

where Q^* is the reactive power reference.

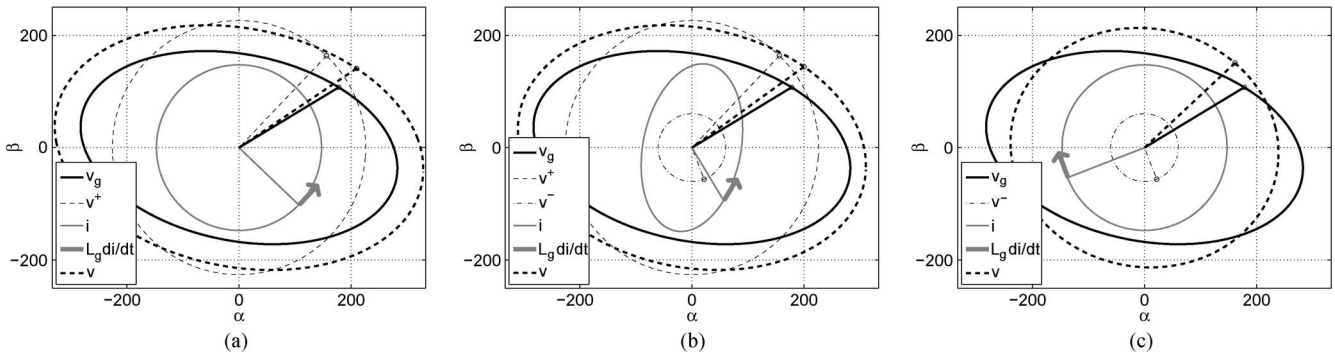

Fig. 3. Voltages and currents in the α–β plane for different voltage support strategies. (a) Following positive sequence. (b) Balancing positive and negative sequences. (c) Following negative sequence.

When the grid is under fault, symmetric sequences (5) and (6) can be introduced in (12)–(15). Due to space limitations, only the reactive current is developed

$$i^*_{\alpha(q)} = \frac{2}{3}Q^* \frac{v^+_\beta + v^-_\beta}{\left(v^+_\alpha + v^-_\alpha\right)^2 + \left(v^+_\beta + v^-_\beta\right)^2} \tag{16}$$

$$i^*_{\beta(q)} = \frac{2}{3}Q^* \frac{-v^+_\alpha - v^-_\alpha}{\left(v^+_\alpha + v^-_\alpha\right)^2 + \left(v^+_\beta + v^-_\beta\right)^2}. \tag{17}$$

Using (7)–(10) into the denominator of (16) and (17)

$$\begin{aligned}&\left(v^+_\alpha + v^-_\alpha\right)^2 + \left(v^+_\beta + v^-_\beta\right)^2 \\ &= \left(v^+_\alpha\right)^2 + \left(v^-_\alpha\right)^2 + 2v^+_\alpha v^-_\alpha + \left(v^+_\beta\right)^2 + \left(v^-_\beta\right)^2 + 2v^+_\beta v^-_\beta \\ &= \left(V^+\right)^2 + \left(V^-\right)^2 + 2V^+V^-\cos(2\omega t + \varphi^+ - \varphi^-).\end{aligned} \tag{18}$$

In (18), an oscillating term appears at twice the grid frequency. This term produces harmonic distortion in the reference currents, and this is the main reason why crossed terms ($2v^+_\alpha v^-_\alpha$ and $2v^+_\beta v^-_\beta$) must disappear whenever low harmonic distortion is mandatory, even in faulted grid conditions. As the first approximation, (16) and (17) should be expressed without crossed terms as

$$i^*_{\alpha(q)} = \frac{2}{3}Q^* \frac{v^+_\beta + v^-_\beta}{\left(v^+_\alpha\right)^2 + \left(v^+_\beta\right)^2 + \left(v^-_\alpha\right)^2 + \left(v^-_\beta\right)^2} \tag{19}$$

$$i^*_{\beta(q)} = \frac{2}{3}Q^* \frac{-v^+_\alpha - v^-_\alpha}{\left(v^+_\alpha\right)^2 + \left(v^+_\beta\right)^2 + \left(v^-_\alpha\right)^2 + \left(v^-_\beta\right)^2}. \tag{20}$$

A. Flexible Balance of Symmetric Sequences

When the reference currents combine a certain amount of positive- and negative-sequence voltages, different results are obtained [23]. Applied to reactive reference current, this balance results in different voltage support strategies. To analyze the voltage support service, the voltage at the PCC can be expressed as

$$v_\alpha = v_{g\alpha} + L_g \frac{di_\alpha}{dt} \tag{21}$$

$$v_\beta = v_{g\beta} + L_g \frac{di_\beta}{dt}. \tag{22}$$

Note that the currents at the input and output sides of the LCL filter are assumed equal, which greatly simplifies the analysis.

The effect of balancing the positive and negative sequences according to (21) and (22) can be graphically interpreted as in Fig. 3. The same voltage sag v_g is represented describing an ellipse in the α–β plane, while positive- and negative-sequence voltages v^+ and v^- describe a circle. Only reactive current is injected to support the grid voltages. Currents are marked in solid gray. These currents can also be decomposed into their positive and negative parts, which are perpendicular to the positive- and negative-sequence voltages, respectively. Their amplitudes depend on the balancing strategy. The current derivative, tangent to that current, is not shown in the graphs; only one instantaneous value is plotted as a thick gray arrow. By projecting this value from the grid voltage, the instantaneous voltage at the PCC, i.e., the voltage support strategy, is obtained. In Fig. 3(a), only the positive sequence is taken into account. As a result, the voltage support strategy matches the voltage sag except that it is larger. Fig. 3(b) shows the balancing of both positive and negative sequences. The result is a combination of voltage rising and voltage equalization. In Fig. 3(c), only the negative voltage sequence is followed, and the result is a highly equalized voltage with low imbalance and phase jump.

It is worth mentioning that phase currents are unbalanced when a combination of positive and negative sequences is used [see Fig. 3(b)]. As a result, the peak current in each phase depends on the strategy used. However, there exist two particular strategies that produce balanced currents (the same peak values in phases a, b, and c), when following only positive-sequence voltage, as shown in Fig. 3(a), or only negative-sequence voltage, as shown in Fig. 3(c).

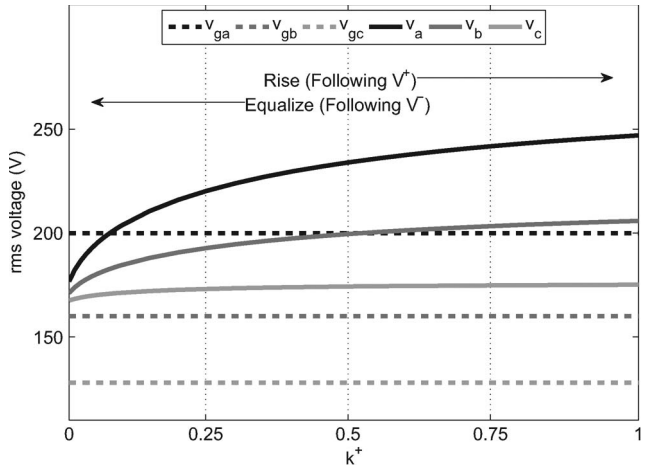

Fig. 4. Voltage support concept as a function of the control parameter k^+.

B. Proposed Control Algorithm

For a flexible voltage support, the balance of positive- and negative-sequence components can be obtained with the following reactive current references:

$$i^*_{\alpha(q)}=\frac{2}{3}Q^*\frac{k^+v^+_\beta+k^-v^-_\beta}{k^+\left[\left(v^+_\alpha\right)^2+\left(v^+_\beta\right)^2\right]+k^-\left[\left(v^-_\alpha\right)^2+\left(v^-_\beta\right)^2\right]} \tag{23}$$

$$i^*_{\beta(q)}=\frac{2}{3}Q^*\frac{-k^+v^+_\alpha-k^-v^-_\alpha}{k^+\left[\left(v^+_\alpha\right)^2+\left(v^+_\beta\right)^2\right]+k^-\left[\left(v^-_\alpha\right)^2+\left(v^-_\beta\right)^2\right]} \tag{24}$$

where k^+ and k^- are the control parameters to balance the positive- and negative-sequence voltages. These control parameters should be normalized, and therefore, the following relation is imposed:

$$k^- = 1 - k^+ \quad | \quad k^+ \in [0,1]. \tag{25}$$

Expressions (23) and (24) present the reference generation for voltage support under grid faults. With this strategy, flexible reactive references are obtained to raise or equalize voltages, and the results in Fig. 3 can be reproduced. The results shown in Fig. 3(a) were obtained by setting $k^+ = 1$ and $k^- = 0$. The voltage support strategy presented in Fig. 3(b) was achieved with $k^+ = k^- = 0.5$. Lastly, the results in Fig. 3(c) were obtained with control parameters $k^+ = 0$ and $k^- = 1$. Different settings of control parameter k^+ produce different voltage support results.

Comparing the conventional (19) and (20) and the proposed control scheme (23) and (24), the conventional control strategy is fixed for different voltage sag characteristics. The proposed control, however, is well suited for balancing positive and negative sequences depending on sag characteristics.

To achieve the desired voltage support service, a proper tuning of k^+ is required. Fig. 4 can help to understand the proposed flexible voltage support concept. In this graph, the rms voltages at the PCC v are compared with the voltages at the grid side v_g for a given voltage sag. By selecting $k^+ \to 1$, the rms voltage will be raised in each phase, although no voltage equalization is achieved. This strategy is well suited for three-phase balanced voltage sags with low negative-sequence component. Basically, in this strategy, the reference currents follow positive-sequence voltages v^+_α, v^+_β. On the contrary, by choosing $k^+ \to 0$, reference currents follow negative-sequence voltages v^-_α, v^-_β. Then, maximum voltage equalization is obtained, but at the expense of less voltage rising. This strategy is of interest in one- or two-phase faults, producing a noticeable negative sequence. In between, a flexible combination of positive- and negative-sequence voltages can be observed with smooth voltage support services. This combination of raising and equalizing strategy is very helpful to avoid disconnection by over- or undervoltage and presents a novel point of view in voltage support control.

In this paper, the basic strategy for active current references is adopted. In this strategy, only positive-sequence voltage is taken into account when generating active reference currents [23]. This strategy is formulated as

$$i^*_{\alpha(p)} = \frac{2}{3}P^*\frac{v^+_\alpha}{\left(v^+_\alpha\right)^2+\left(v^+_\beta\right)^2} \tag{26}$$

$$i^*_{\beta(p)} = \frac{2}{3}P^*\frac{v^+_\beta}{\left(v^+_\alpha\right)^2+\left(v^+_\beta\right)^2}. \tag{27}$$

Note that, depending on grid codes and the depth of the voltage sag, the active current $i^*_{\alpha(p)}, i^*_{\beta(p)}$ can be set to zero [33]. If not, regulations dictate the ratio between active and reactive currents to keep feeding the grid. These active currents have no noticeable effect on the voltage support.

The complete reference currents are the sum of active and reactive currents

$$i^*_\alpha = i^*_{\alpha(p)} + i^*_{\alpha(q)} \tag{28}$$

$$i^*_\beta = i^*_{\beta(p)} + i^*_{\beta(q)}. \tag{29}$$

The proposed control scheme, presented in (23)–(29), ensures the following.

1) By proper tuning of one single control parameter k^+ ($k^- = 1 - k^+$), the voltage at the inverter side can be raised ($k^+ \to 1$), equalized ($k^+ \to 0$), or a flexible combination of both ($0 < k^+ < 1$).
2) No harmonic distortion appears in the references because the crossed terms in positive and negative sequences have been eliminated.
3) Instantaneous active power, averaged over one grid cycle, equals the reference, i.e., $\int p(t)dt = P^*$.
4) The same applies to instantaneous reactive power, i.e., $\int q(t)dt = Q^*$.

IV. Theoretical Analysis

This section analyzes the behavior of the voltage support control scheme proposed in Section III-B under grid faults. A theoretical interpretation of peak currents, active and reactive instantaneous powers, and voltage support is provided.

In order to analyze these results, some assumptions are needed

$$i_\alpha \approx i^*_\alpha \qquad i_\beta \approx i^*_\beta \tag{30}$$

$$\Delta\varphi^+ \approx 0 \qquad \Delta\varphi^- \approx 0. \tag{31}$$

The first assumption (30) states that the output currents follow their references. This assumption is reasonable in steady-state operation of the inverter. The second assumption (31) indicates that there is no variation in the initial phase jump, which is not true in most voltage sags, but if the angle is small, the approximations can be assumed without loss of generality.

A. Peak Currents

To keep currents within safety values, a detailed analysis must be performed. The inverter can inject active and/or reactive power, and the currents in each phase can be unbalanced, as stated in Section III-A. These peak amplitudes must be taken under consideration to avoid overcurrent problems. Substituting (7)–(10) into (23)–(27), the inverter currents can be expressed as

$$i_\alpha^+ = \frac{2}{3}P^* \frac{1}{V^+}\cos(\omega t) \tag{32}$$

$$i_\alpha^- = \frac{2}{3}Q^* \frac{k^+V^+ - k^-V^-}{k^+(V^+)^2 + k^-(V^-)^2}\sin(\omega t) \tag{33}$$

$$i_\beta^+ = \frac{2}{3}P^* \frac{1}{V^+}\sin(\omega t) \tag{34}$$

$$i_\beta^- = \frac{2}{3}Q^* \frac{-k^+V^+ - k^-V^-}{k^+(V^+)^2 + k^-(V^-)^2}\cos(\omega t). \tag{35}$$

Note that i_α^+ and i_β^+ have the same peak value. However, in the case of negative-sequence current, the amplitudes are different in the α and β channels.

From (32)–(35), current amplitudes in each phase I_a, I_b, and I_c can be obtained. These amplitudes depend on control parameters, and active and reactive power references. They are computed using the inverse Clarke transformation of $i_\alpha = i_\alpha^+ + i_\alpha^-$ and $i_\beta = i_\beta^+ + i_\beta^-$ and then obtaining the module

$$I_a = \sqrt{(xP^*)^2 + (yQ^*)^2} \tag{36}$$

$$I_b = \frac{1}{2}\sqrt{\left(-xP^* + \sqrt{3}zQ^*\right)^2 + \left(-yQ^* + \sqrt{3}xP^*\right)^2} \tag{37}$$

$$I_c = \frac{1}{2}\sqrt{\left(-xP^* - \sqrt{3}zQ^*\right)^2 + \left(-yQ^* - \sqrt{3}xP^*\right)^2} \tag{38}$$

where

$$x = \frac{2}{3}\frac{1}{V^+} \tag{39}$$

$$y = \frac{2}{3}\frac{k^+V^+ - k^-V^-}{k^+(V^+)^2 + k^-(V^-)^2} \tag{40}$$

$$z = \frac{2}{3}\frac{-k^+V^+ - k^-V^-}{k^+(V^+)^2 + k^-(V^-)^2}. \tag{41}$$

B. Instantaneous Power

According to Yazdani and Iravani [39], the active and reactive instantaneous powers are

$$p = \frac{3}{2}(v_\alpha i_\alpha + v_\beta i_\beta) \tag{42}$$

$$q = \frac{3}{2}(-v_\alpha i_\beta + v_\beta i_\alpha). \tag{43}$$

When the three-phase voltages are balanced, the instantaneous active and reactive powers obtained by implementing the conventional control scheme of (12)–(15) are $p = P^*$ and $q = Q^*$. In this ideal scenario, no oscillation is obtained neither in the active power nor in the reactive power. However, in unbalanced grid conditions, the instantaneous powers oscillate at twice the grid frequency $p = P^* + \tilde{p}$ and $q = Q^* + \tilde{q}$ [17]–[23]. It is worth mentioning that the oscillating terms $\tilde{p}$ and $\tilde{q}$ have no dc component.

Equations (42) and (43) can be decomposed into positive and negative components and oscillating terms at twice the grid frequency. Substituting (7)–(10) and (23)–(27) in (42) and (43)

$$p^+ = \frac{3}{2}\left(v_\alpha^+ i_\alpha^+ + v_\beta^+ i_\beta^+\right) = P^* \tag{44}$$

$$p^- = \frac{3}{2}\left(v_\alpha^- i_\alpha^- + v_\beta^- i_\beta^-\right) = 0 \tag{45}$$

$$\begin{aligned}\tilde{p} &= \frac{3}{2}\left(v_\alpha^+ i_\alpha^- + v_\beta^+ i_\beta^- + v_\alpha^- i_\alpha^+ + v_\beta^- i_\beta^+\right)\\ &= nP^*\cos(2\omega t) + \frac{k^+ - k^-}{k^+ + n^2k^-}nQ^*\sin(2\omega t)\end{aligned} \tag{46}$$

$$q^+ = \frac{3}{2}\left(-v_\alpha^+ i_\beta^+ + v_\beta^+ i_\alpha^+\right) = \frac{k^+}{k^+ + n^2k^-}Q^* \tag{47}$$

$$q^- = \frac{3}{2}\left(-v_\alpha^- i_\beta^- + v_\beta^- i_\alpha^-\right) = \frac{n^2k^-}{k^+ + n^2k^-}Q^* \tag{48}$$

$$\begin{aligned}\tilde{q} &= \frac{3}{2}\left(-v_\alpha^+ i_\beta^- + v_\beta^+ i_\alpha^- - v_\alpha^- i_\beta^+ + v_\beta^- i_\alpha^+\right)\\ &= -nP^*\sin(2\omega t) + \frac{1}{k^+ + n^2k^-}nQ^*\cos(2\omega t).\end{aligned} \tag{49}$$

From (44) and (45), active power is transferred via positive-sequence power p^+, as formulated in (26) and (27). The negative-sequence power p^- is zero. However, from (47) and (48), reactive power has positive q^+ and negative q^- sequences since the proposed control balances these values using the control parameter k^+. Note that the sum of positive and negative reactive powers is $q^+ + q^- = Q^*$.

In (46) and (49), oscillating terms appear at twice the grid frequency both in the active $\tilde{p}$ and reactive $\tilde{q}$ powers. These oscillations are proportional to the voltage unbalance factor. However, when $k^+ = k^- = 0.5$, the oscillation in p due to Q^* is minimized because the term containing $k^+ - k^-$ vanishes. This strategy is interesting in unbalanced grid faults because it can either raise or equalize voltage with low dc-link voltage oscillations.

C. Voltage Support

Resuming (21) and (22) for reactive currents, by substitution of (32)–(35), positive V^+ and negative V^- sequence amplitudes at the inverter side are calculated

$$V^+ = V_g^+ + \frac{2}{3}Q^*\frac{\omega L_g V^+ k^+}{k^+(V^+)^2 + k^-(V^-)^2} \tag{50}$$

$$V^- = V_g^- - \frac{2}{3}Q^*\frac{\omega L_g V^- k^-}{k^+(V^+)^2 + k^-(V^-)^2}. \tag{51}$$

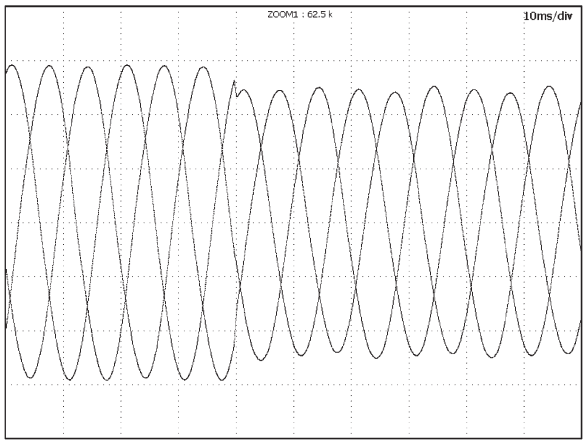

Fig. 5. Test 1: Grid voltage (100 V/div.) for the type-A voltage sag.

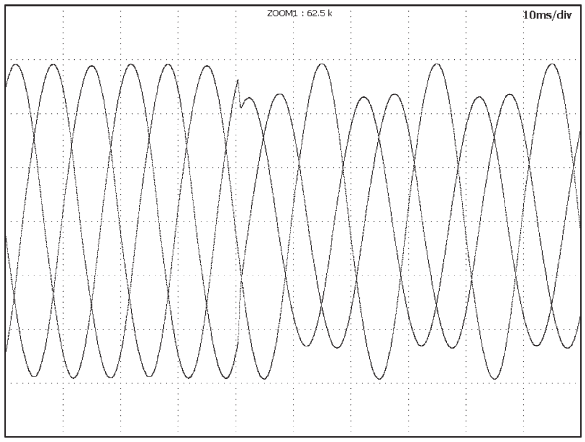

Fig. 6. Test 2: Grid voltage (100 V/div.) for the type-C voltage sag.

When setting control parameter $k^+ \to 1$, the positive-sequence magnitude increases while the negative-sequence magnitude remains unchanged. In a similar way, by setting $k^+ \to 0$, the positive sequence is kept constant, but the negative sequence decreases.

Limitations of this method have to do with the maximum allowed current and the value of grid inductance. An inverter with higher rated power can inject higher reactive current. As a result, better voltage support is obtained.

It is worth mentioning that the proposed control scheme can help the grid by supporting its voltage in both stiff and weak grids. However, in the case of stiff grids, the voltage support results are small regardless of the control strategy implemented. In weak grids, the voltage support is more significant.

V. Numerical Example

In order to evaluate the control proposal, two different voltage sags [30] have been tested.

1) Test 1 is a balanced three-phase voltage sag (type A).
2) Test 2 is a single-phase-to-ground voltage sag (type C).

Their waveforms are shown in Figs. 5 and 6, respectively. Both sags have been characterized in detail. In Table I, the p.u. values are presented (1 p.u. $= 200\sqrt{2}$ V).

TABLE I
Voltage Sag Characterization

	Before sag	**Sag test 1**	**Sag test 2**
$v_{g(a)}$	$1.000\angle 0°$	$0.855\angle 0°$	$1.025\angle 0°$
$v_{g(b)}$	$1.010\angle -117°$	$0.840\angle -128°$	$0.780\angle -133°$
$v_{g(c)}$	$1.010\angle 122°$	$0.830\angle 118°$	$0.820\angle 132°$
V_g^+	1.001	0.840	0.862
V_g^-	0.016	0.042	0.182

A. Test 1

In test 1, the voltage sag is characterized by $V_g^+ = 0.840$ p.u. and $V_g^- = 0.042$ p.u. The expected theoretical power characteristics for a control strategy $k^+ = 0.9$ are developed. It is assumed that active and reactive power references are set to $P^* = 2750$ W and $Q^* = 3000$ var, and system parameters are $\omega = 2\pi 50$ rad/s and $L_g = 5$ mH.

Applying (50) and (51), theoretical values of $V^+ = 0.885$ p.u. and $V^- = 0.042$ p.u. are obtained. These results indicate that the positive-sequence magnitude is greater than the initial one while the negative remains more or less unchanged, as stated in Section IV-C for $k^+ \to 1$.

Peak currents are obtained from (36)–(38). The results are $I_a = 7.65\sqrt{2}$ A, $I_b = 7.70\sqrt{2}$ A, and $I_c = 7.66\sqrt{2}$ A. Also, as explained before, the currents are nearly balanced for $k^+ = 0.9$.

Maximum oscillations in active and reactive powers are obtained by substituting for this strategy in (42) and (43). The peak-to-peak oscillations are $\tilde{p} = 360$ W and $\tilde{q} = 405$ var. In this type of voltage sag, the unbalance factor n is low, and therefore, low-power oscillations appear in the system.

B. Test 2

Another numerical example is analyzed for test 2. The voltage sag is characterized by $V_g^+ = 0.862$ p.u. and $V_g^- = 0.182$ p.u. The control strategy has been selected at $k^+ = 0.5$. For this case, the active and reactive power references are set to $P^* = 1000$ W and $Q^* = 2750$ var.

The expected theoretical values of positive- and negative-sequence amplitudes are $V^+ = 0.901$ p.u. and $V^- = 0.174$ p.u., so the voltage unbalance factor has been corrected from $n = 0.211$ to $n = 0.193$. These results indicate that the voltage imbalance can be corrected when balancing positive- and negative-sequence voltages in the proposed strategy.

To get the peak currents values, the same procedure is followed. The resulting values are $I_a = 4.37\sqrt{2}$ A, $I_b = 6.00\sqrt{2}$ A, and $I_c = 5.48\sqrt{2}$ A. In the previous numerical example, the peak currents were similar in each phase because the control parameter tends to $k^+ \to 1$. However, when setting flexible combinations of positive- and negative-sequence voltages $0 < k^+ < 1$, the current peak values are different for each phase.

Power oscillations in active power are quite low $\tilde{p} = 387$ W because, in this strategy, $k^+ = k^-$, and the oscillation in p due to reactive power is zero. On the other hand, the oscillation in the reactive power is high $\tilde{q} = 2085$ var.

TABLE II
SYSTEM PARAMETERS

	Symbol	Nominal value
dc-link voltage	v_{dc}	650 V
inverter inductor	L_i	5 mH
filter capacitor	C	680 nF
damping resistor	r_d	6.8 Ω
output inductor	L_o	2 mH
grid inductor	L_g	5 mH
grid voltage	v_g	200 V, 50 Hz
switching frequency	f_s	10 kHz

VI. EXPERIMENTAL RESULTS

A test platform was built using an Amrel SPS-800-12 dc power source configured as a photovoltaic panel emulator, a 4.5-kVA Semikron three-phase insulated-gate bipolar transistor bridge, and a Chroma 61704 ac power source to emulate the grid and get repetitive faults. To absorb active power, a 4000-W resistive load is employed. For voltage support, an inductor between PCC and the voltage source is used. The control algorithm is implemented on a Texas Instruments TMS320F28335 floating point digital signal processor. Nominal values of the system parameters are collected in Table II.

In test 1, a balanced three-phase voltage sag (type A) is programmed. In test 2, a single-phase-to-ground (type C) sag is tested. Previously, in Section V, the two selected voltage sags were characterized in Table I.

During the experiments, each test analyzes four different control strategies lasting 0.1 s. The voltage sag occurs at time $t = 0$. In the interval $0 \leq t < 0.1$ s, no voltage support is programmed (i.e., no reactive current is injected $i^*_{\alpha(q)} = 0$ and $i^*_{\beta(q)} = 0$); only the control strategy shown in (26) and (27) is implemented. Thus, the magnitude and effects of the voltage sag can be explicitly shown. After that, $0.1 \leq t < 0.2$ s, the control parameter is set to $k^+ = 0.9$. This policy is well suited for balanced voltage sags when no appreciable negative sequence is present. In the next strategy, $0.2 \leq t < 0.3$ s, k^+ is set to 0.5. Minimal active power oscillations are appreciable while increasing and equalizing the voltage. The last policy, $0.3 \leq t < 0.4$ s, changes the controller parameter to $k^+ = 0.1$. This strategy is very useful to reduce negative-sequence voltage, particularly in unbalanced grid faults. The sag takes 0.4 s to vanish; although not shown in the experiments, the voltage values return to the prefaulted rated values.

Fig. 7 shows a control diagram of the voltage support strategy implemented in this study. This diagram is composed of a sag detector and a two-input multiplexer. The output of the sag detector drives the multiplexer which provides the parameters Q^*, k^+, and k^- according to the values listed in Table III. This table lists the reference values of the active and reactive powers used in the experiments. The values correspond to various operating points computed offline to show experimentally the voltage support characteristics of the proposed control scheme. Different values are obtained for each test and for each control parameter k^+. To obtain these values, extensive simulations have been carried out in order to obtain safety peak currents.

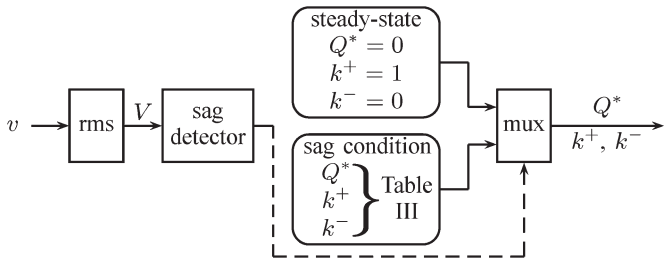

Fig. 7. Control diagram of the implemented voltage support control.

TABLE III
ACTIVE P^* (IN WATTS) AND REACTIVE Q^* (IN VARS) POWER REFERENCES

	Test 1	Test 2	Time(s)	Strategy
P^*	2750	1000	$[-0.1, 0.4)$	feed the grid
Q^*	0	0	$[-0.1, 0.1)$	no voltage support
Q^*	3000	3000	$[0.1, 0.2)$	$k^+ = 0.9$
Q^*	3000	2750	$[0.2, 0.3)$	$k^+ = 0.5$
Q^*	2500	1400	$[0.3, 0.4)$	$k^+ = 0.1$

TABLE IV
CONTROL PARAMETERS

	Symbol	Value
SOGI sequence extractor		
damping factor	ξ_s	$\frac{\sqrt{2}}{2}$
current control		
selected harmonics to be attenuated	m	{1,5,7,11}
damping factor	ξ	0.1
proportional gain	k_p	30
resonant gain	k_r	150
dc-link voltage regulator		
dc-link reference	v^*_{dc}	650 V
proportional gain	$k_{p\,dc}$	5
intregral gain	$k_{i\,dc}$	30

Due to hardware limitations, positive and negative magnitudes cannot achieve the targets $V^+ = 1$ p.u. and $V^- = 0$ p.u, respectively. These optimal targets assume that voltage at the inverter side corresponds to normal values during grid fault. Bigger inductors and more available current will help support the grid voltage. At any rate, the experimental section tries to clearly show tendencies instead of absolute values.

Three main control algorithms are implemented in this work: the symmetric sequence extractor, the current loop, and the dc-link voltage regulator. The values of the control parameters are collected in Table IV. The sequence extractor used in this work is the second-order generalized integrator reported in [37]. Interesting design guideline and digital implementation can be found in [38]. It implements an adaptive bandpass filter tuned at the fundamental grid frequency ω to reject voltage harmonics $\widehat{v}$ and a low-pass filter to obtain its filtered quadrature $\widehat{v}_q$, in both α and β voltage channels. The filters are frequency adaptive $\widehat{\omega}$ because they use a frequency

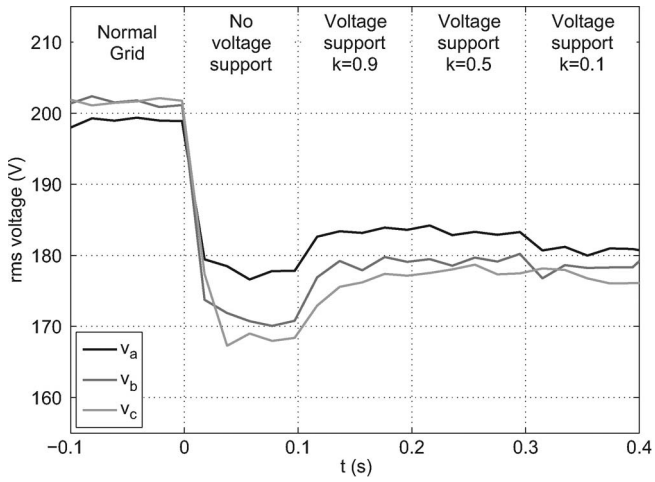

Fig. 8. Test 1: PCC rms voltages.

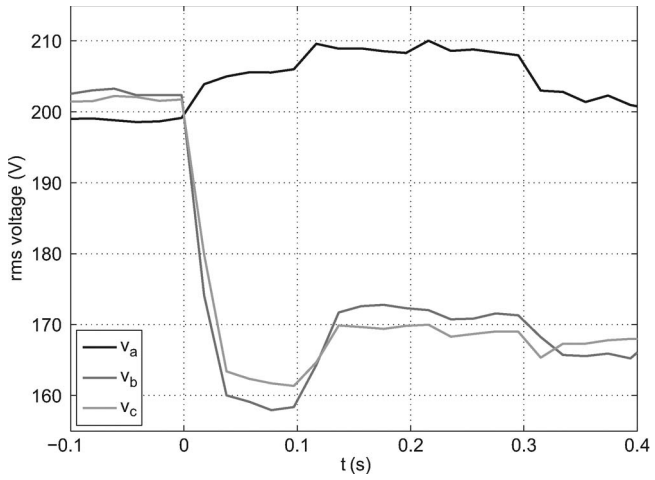

Fig. 9. Test 2: PCC rms voltages.

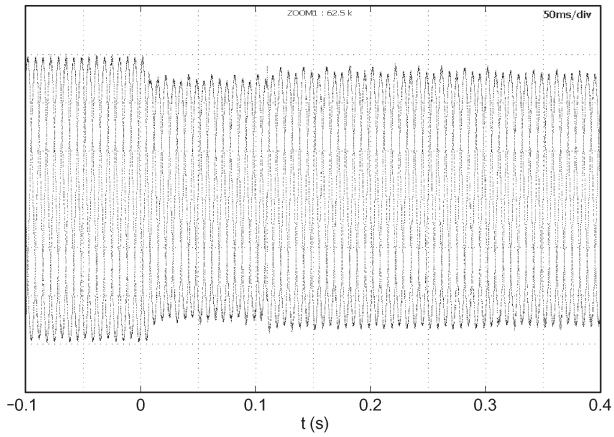

Fig. 10. Test 1: PCC voltage waveforms (100 V/div.).

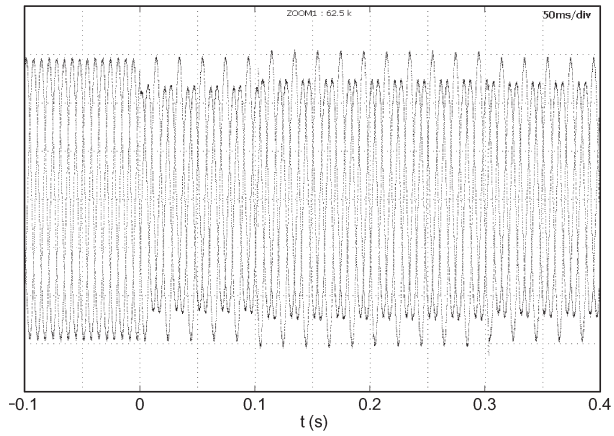

Fig. 11. Test 2: PCC voltage waveforms (100 V/div.).

locked loop. In the Laplace s domain, the implemented transfer functions are

$$\frac{\widehat{v}(s)}{v(s)} = \frac{2\xi_s \widehat{\omega} s}{s^2 + 2\xi_s \widehat{\omega} s + \widehat{\omega}^2} \tag{52}$$

$$\frac{\widehat{v_q}(s)}{v(s)} = \frac{2\xi_s \widehat{\omega}^2}{s^2 + 2\xi_s \widehat{\omega} s + \widehat{\omega}^2}. \tag{53}$$

It is worth mentioning that the reaction time of the proposed control scheme mainly relies on the sequence extractor. According to the values listed in Table IV, the reaction time of the implemented sequence extractor is one and a half grid period, resulting in a fast system transient response.

Another important implementation issue is the current control loop to accurately track the generated references. In this paper, a proportional resonant current controller with a harmonic compensator is implemented for this purpose [40]. The interested reader can find a stability analysis of this loop therein.

The current controller implements the following transfer function:

$$H(s) = k_p + \sum_{m=1,5,7,11} \frac{k_r 2\xi(m\omega)s}{s^2 + 2\xi(m\omega)s + (m\omega)^2} \tag{54}$$

where k_p is the proportional gain, k_r is the resonant gain, ξ is the damping factor, and m is the selected harmonics to be attenuated.

The dc-link voltage regulator includes a proportional–integral compensator and a notch filter tuned at twice the grid frequency [39] to ensure high rejection of current harmonics caused by unbalanced grid conditions.

During the experiments, high-frequency noise has been filtered in order to better show the voltage support services.

A. PCC Voltage

RMS phase voltages at the PCC for the two selected voltage sags are shown in Figs. 8 and 9. Voltage waveforms are included in Figs. 10 and 11.

Before the fault, the voltage in each phase is around 200 V. At time $t = 0$ s, the voltage sag occurs. At time $t = 0.1$ s, the voltage support strategy is activated. First, the control parameter k^+ is set to 0.9. Then, at $t = 0.2$ s, it changes to 0.5. Finally, at $t = 0.3$ s, the parameter is set to 0.1 in order to compare the flexible properties of the proposed voltage support control scheme.

The preferred voltage support strategy for test 1 occurs with $k^+ \to 1$ because no appreciable voltage imbalance exists in type-A sags. In this type of grid fault, only a rising strategy

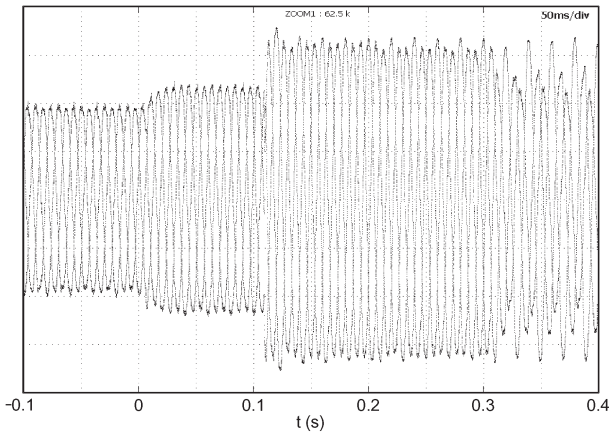

Fig. 12. Test 1: Output currents (3.2 A/div.).

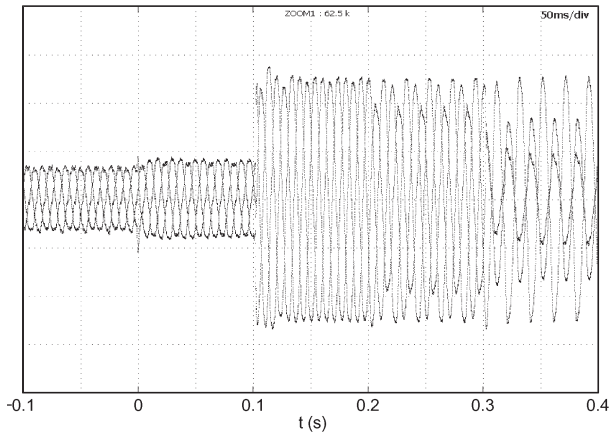

Fig. 13. Test 2: Output currents (3.2 A/div.).

makes sense because the rms voltage is almost equal in all the phases, and all the phases need to be recovered. Overvoltage is rarely a problem in balanced voltage sags.

In test 2, a type-C voltage sag is experienced. One phase remains unchanged while the other two suffer the fault. When setting $k^+ = 0.9$, the voltages in all three phases are increased without equalization. The problem with this strategy is that, eventually, the voltage in phase a can exceed the overvoltage limit and cause system disconnection. Thus, voltage equalization avoids this undesirable phenomenon at the expense of less voltage rising. As $k^+ \to 0$, more equalization is obtained, which can help to ride through unbalanced voltage sags.

In these two figures, it is clearly shown that balanced voltage sags require a different strategy than unbalanced two-phase faults. In type-A sags, disconnection by overvoltage is extremely rare and can always be compensated by reducing the reactive power reference. However, in type-C voltage sags, a balance between rising and equalization needs to be implemented; then, overvoltage in the phase that does not suffer the sag can be avoided while increasing the rms voltage in the other phases above regulation limits.

B. Current

The output current waveforms in the two experiments are shown in Figs. 12 and 13.

In test 1, the currents in each phase before the fault are approximately $4.5\sqrt{2}$ A. When the fault occurs, the grid voltage is reduced. In the first strategy, only the active power is injected into the grid in the time interval $0 \leq t < 0.1$ s. Therefore, to keep active power balance, the currents increase to $5.4\sqrt{2}$ A. After that time, the voltage support is activated. Reactive power references are changed in each strategy so as to keep peak currents just below the tripping-out values. The same reasoning applies to test 2, although lower active power and trip-out current have been selected.

In both cases, if the control parameter is set to $k^+ \to 1$, the currents are balanced, but in the case $k^+ = 0.5$ and even more when $k^+ = 0.1$, the currents in phases a, b, and c are unbalanced, as discussed in Section III-A.

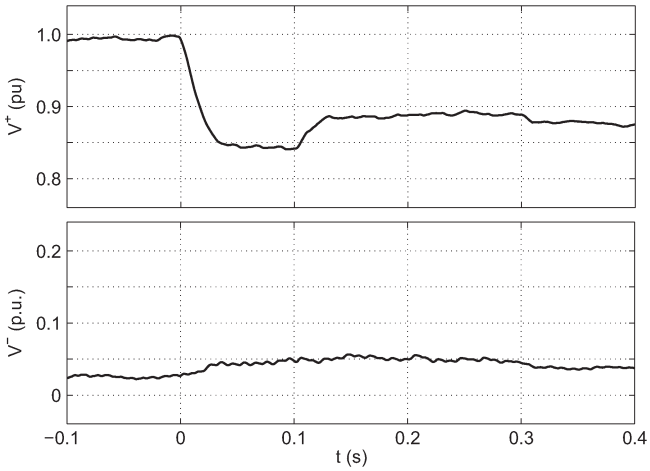

Fig. 14. Test 1: Positive V^+ and negative V^- sequence amplitudes.

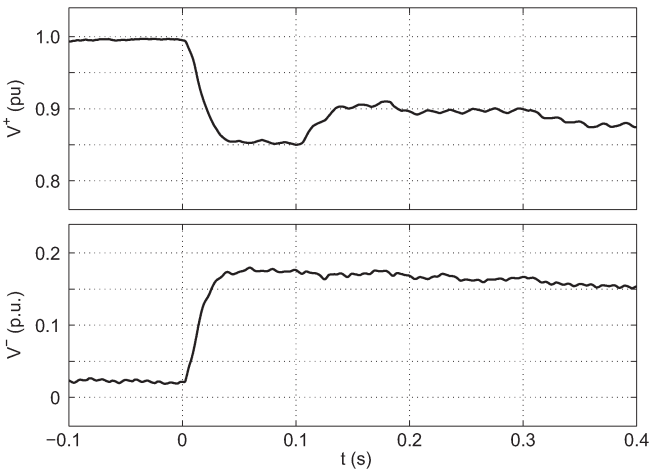

Fig. 15. Test 2: Positive V^+ and negative V^- sequence amplitudes.

C. Positive and Negative Sequences

Figs. 14 and 15 show the amplitude of the positive- and negative-sequence voltages at the PCC. Note that the reaction time is only one and a half grid period. In balanced sags (test 1), the negative sequence is almost negligible. As k^+ increases, so does the positive sequence.

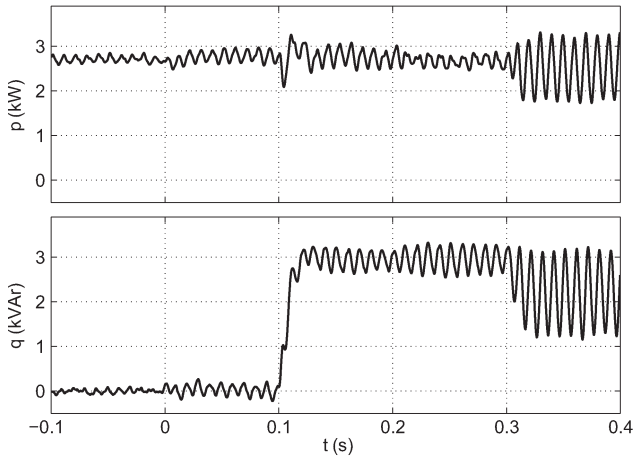

Fig. 16. Test 1: Active p and reactive q powers.

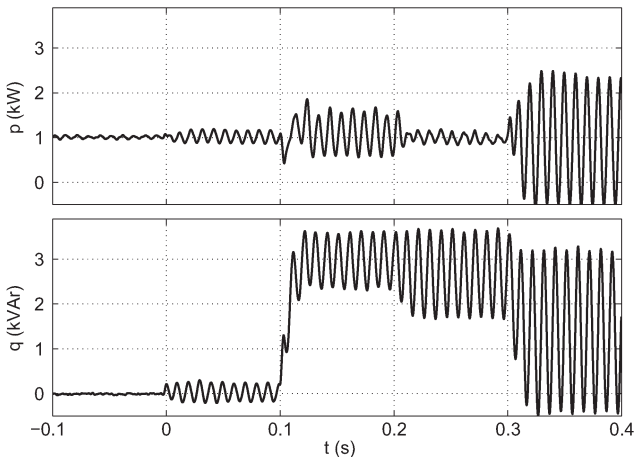

Fig. 17. Test 2: Active p and reactive q powers.

In single phase to ground (test 2), the negative sequence is noticeable but can be reduced by decreasing k^+. As $k^+ \to 0$, the negative sequence $V^- \to 0$.

With the proposed control scheme, it is possible to easily and independently increase the positive sequence by setting $k^+ \to 1$ or decrease the negative sequence by setting $k^+ \to 0$. It should be noted that the reduction of the voltage unbalance factor allows for better performance of three-phase DG inverters [13].

D. Active and Reactive Instantaneous Powers

The measured active and reactive powers are shown in Figs. 16 and 17. The upper part of each graph presents the active power, while the lower part of each graph shows the reactive power.

These figures show that the reference generator can independently track the active and reactive powers P^* and Q^* collected in Table III.

A negative sequence induces an oscillation in the active and reactive powers, as analyzed in Section IV-B. The oscillation appears at twice the grid frequency. Different amplitudes are obtained for different control parameters. If the control parameter is set to $k^+ = k^- = 0.5$, the oscillation in the active power is always minimized, and therefore, this could be a good solution whenever no extreme voltage sags are experienced. Also, this strategy balances both rising and equalizing properties.

It is worth mentioning that the experimental results agree with the expected theoretical values.

VII. Conclusion

A flexible voltage support control scheme has been proposed in this paper for three-phase DG inverters under a grid fault. The voltage support strategy can be modified by means of a control parameter according to the type of voltage sag. In three-phase balanced sags, the best solution seems to be to raise the voltage in all phases by selecting k^+ near to one. In one- or two-phase faults, voltage equalization is a preferred choice because conventional strategies can lead to overvoltage and cause disconnection. When the sag is very deep, k^+ should be near to zero; when the sag is less deep, a balance between these two extreme policies should be implemented.

The proposed voltage support control scheme has the following advantages: 1) flexibly support the grid voltage; 2) increase positive or decrease negative voltage sequence; and 3) clear the phase jump, which is a powerful tool for voltage support.

A detailed analysis has been developed in order to theoretically describe the behavior of the proposed voltage support control.

Two different scenarios have been experimentally tested to illustrate the results of the proposed voltage support control with a flexible combination of rising and equalizing capabilities. Selected experimental tests confirm the theoretical features of this control algorithm.

Future work will be focused on the run-time tuning of the controller to achieve particular control objectives and a detailed design guideline to comply with specific grid codes. Also, a voltage support control loop should be developed and compared with other control architectures.

References

[1] "L'Observatoire des Energies Renouvelables. Systemes solaires (Observ'er): Wind power barometer," *le Journal de L'eolien*, Rep., Feb. 2011.

[2] "Trends in photovoltaic applications. Survey peport of selected IEA countries between 1992 and 2007," Photovoltaic Power Systems Programme. IEA Int. Energy Agency, St. Ursen, Switzerland, Aug. 2008.

[3] "New ERA for electricity in Europe. Distributed generation: Key issues, challenges and proposed solutions," Eur. Commission, Energy Prod. Distrib. Syst., Brussels, Belgium, 2003.

[4] R. Lasseter, A. Akhil, C. Marnay, J. Stephens, J. Dagle, R. Guttromson, A. S. Meliopoulous, R. Yinger, and J. Eto, "White paper on integration of distributed energy resources. The CERTS microgrid concept," Consortium for Electric Reliability Technology Solutions, Berkeley, CA, 2002.

[5] J. M. Guerrero, J. Matas, L. G. de Vicuna, M. Castilla, and J. Miret, "Decentralized control for parallel operation of distributed generation inverters using resistive output impedance," *IEEE Trans. Ind. Electron.*, vol. 54, no. 2, pp. 994–1004, Apr. 2007.

[6] "Towards smart power networks. Lessons learned from European research FP5 projects. EUR 21970," Eur. Commission, Brussels, Belgium, 2005.

[7] J. M. Guerrero, J. C. Vasquez, J. Matas, L. G. de Vicuna, and M. Castilla, "Hierarchical control of droop-controlled AC and DC microgrids. A general approach towards standardization," *IEEE Trans. Ind. Electron.*, vol. 58, no. 1, pp. 158–172, Jan. 2011.

[8] B. Kirby and E. Hirst, "Ancillary-service details: Voltage control," Oak Ridge Nat. Lab., Oak Ridge, TN, Tech. Rep. ORNL/CON-453, Dec. 1997.

[9] S. Kincic, X. Wan, D. McGillis, A. Chandra, B.-T. Ooi, F. Galiana, and G. Joos, "Voltage support by distributed static VAr systems (SVS)," *IEEE Trans. Power Del.*, vol. 20, no. 2, pp. 1541–1549, Apr. 2005.

[10] M. Tsili and S. Papathanassiou, "A review of grid code technical requirements for wind farms," *IET Renewable Power Gener.*, vol. 3, no. 3, pp. 308–332, Sep. 2009.
[11] F. Iov, A. D. Hansen, P. Sorensen, and N. A. Cutululis, "Mapping of grid faults and grid codes," Riso Nat. Lab., Techn. Univ. Denmark, Roskilde, Denmark, Tech. Rep., 2007.
[12] *Characteristics of the Utility Interface for Photovoltaic Systems*, IEC Std. 61727-2002, 2002.
[13] A. von Jouanne and B. Banerjee, "Assessment of voltage unbalance," *IEEE Trans. Power Del.*, vol. 16, no. 4, pp. 782–790, Oct. 2001.
[14] *IEEE Application guide for IEEE Std. 1547, IEEE Standard for Interconnecting Distributed Resources With Electric Power Systems*, IEEE Std. 1547.2-2008, 2008.
[15] P. Rioual, H. Pouliquen, and J.-P. Louis, "Regulation of a PWM rectifier in the unbalanced network state using a generalized model," *IEEE Trans. Power Electron.*, vol. 11, no. 3, pp. 495–502, May 1996.
[16] B. Yin, R. Oruganti, S. K. Panda, and A. K. S. Bhat, "An output-power-control strategy for a three-phase PWM rectifier under unbalanced supply conditions," *IEEE Trans. Ind. Electron.*, vol. 55, no. 5, pp. 2140–2151, May 2008.
[17] P. Rodriguez, A. Timbus, R. Teodorescu, M. Liserre, and F. Blaabjerg, "Flexible active power control of distributed power generation systems during grid faults," *IEEE Trans. Ind. Electron.*, vol. 54, no. 5, pp. 2583–2592, Oct. 2007.
[18] P. Rodriguez, A. Timbus, R. Teodeorescu, M. Liserre, and F. Blaabjerg, "Independent PQ control for distributed power generation systems under grid faults," in *Proc. 32nd IEEE Annu. Conf. Ind. Electron.*, Nov. 2006, pp. 5185–5190.
[19] S. Alepuz, S. Busquets-Monge, J. Bordonau, J. Martinez-Velasco, C. Silva, J. Pont, and J. Rodriguez, "Control strategies based on symmetrical components for grid-connected converters under voltage dips," *IEEE Trans. Ind. Electron.*, vol. 56, no. 6, pp. 2162–2173, Jun. 2009.
[20] I. Etxeberria-Otadui, U. Viscarret, M. Caballero, A. Rufer, and S. Bacha, "New optimized PWM VSC control structures and strategies under unbalanced voltage transients," *IEEE Trans. Ind. Electron.*, vol. 54, no. 5, pp. 2902–2914, Oct. 2007.
[21] F. Wang, J. Duarte, and M. Hendrix, "Design and analysis of active power control strategies for distributed generation inverters under unbalanced grid faults," *IET Gener., Transmiss. Distrib.*, vol. 4, no. 8, pp. 905–916, Aug. 2010.
[22] F. Wang, J. L. Duarte, and M. A. M. Hendrix, "Pliant active and reactive power control for grid-interactive converters under unbalanced voltage dips," *IEEE Trans. Power Electron.*, vol. 26, no. 5, pp. 1511–1521, May 2011.
[23] M. Castilla, J. Miret, J. Sosa, J. Matas, and L. G. de Vicuna, "Grid-fault control scheme for three-phase photovoltaic inverters with adjustable power quality characteristics," *IEEE Trans. Power Electron.*, vol. 25, no. 12, pp. 2930–2940, Dec. 2010.
[24] M. Altin, O. Goksu, R. Teodorescu, P. Rodriguez, B.-B. Jensen, and L. Helle, "Overview of recent grid codes for wind power integration," in *Proc. 12th Int. Conf. Optim. Elect. Electron. Equipment*, May 2010, pp. 1152–1160.
[25] F. Blaabjerg, R. Teodorescu, M. Liserre, and A. Timbus, "Overview of control and grid synchronization for distributed power generation systems," *IEEE Trans. Ind. Electron.*, vol. 53, no. 5, pp. 1398–1409, Oct. 2006.
[26] M. Liserre, F. Blaabjerg, and S. Hansen, "Design and control of an LCL-filter-based three-phase active rectifier," *IEEE Trans. Ind. Appl.*, vol. 41, no. 5, pp. 1281–1291, Sep./Oct. 2005.
[27] E. Figueres, G. Garcera, J. Sandia, F. Gonzalez-Espin, and J. Rubio, "Sensitivity study of the dynamics of three-phase photovoltaic inverters with an LCL grid filter," *IEEE Trans. Ind. Electron.*, vol. 56, no. 3, pp. 706–717, Mar. 2009.
[28] *IEEE Recommended Practice for Monitoring Electric Power Quality*, IEEE Std. 1159-1995, 1995.
[29] M. McGranaghan, D. Mueller, and M. Samotyj, "Voltage sags in industrial systems," *IEEE Trans. Ind. Appl.*, vol. 29, no. 2, pp. 397–403, Mar./Apr. 1993.
[30] M. Bollen, "Characterisation of voltage sags experienced by three-phase adjustable-speed drives," *IEEE Trans. Power Del.*, vol. 12, no. 4, pp. 1666–1671, Oct. 1997.
[31] A. Sannino, M. Bollen, and J. Svensson, "Voltage tolerance testing of three-phase voltage source converters," *IEEE Trans. Power Del.*, vol. 20, no. 2, pp. 1633–1639, Apr. 2005.
[32] M. Fontela, S. Bacha, N. Hadjsaid, and C. Andrieu, "Functional specifications of electric networks with high degrees of distributed generation," CRISP, Distributed Intelligence in Critical Infrastructures for Sustainable Power. INPGrenoble/Schneider Electric, Lyon, France, Tech. Rep., 2003.
[33] Red Electrica (REE), Operat. Proced., Resolution-P.O.12.3—Response Requirements Against Voltage Dips in Wind Installations, Oct. 2006.
[34] P. Rodriguez, J. Pou, J. Bergas, J. I. Candela, R. P. Burgos, and D. Boroyevich, "Decoupled double synchronous reference frame PLL for power converters controls," *IEEE Trans. Power Electron.*, vol. 22, no. 2, pp. 584–592, Mar. 2007.
[35] F. Neves, H. Souza, E. Bueno, M. Rizo, F. Bradaschia, and M. Cavalcanti, "A space-vector discrete Fourier transform for detecting harmonic sequence components of three-phase signals," in *Proc. 35th Annu. Conf. IEEE Ind. Electron.*, Nov. 2009, pp. 3631–3636.
[36] G. Saccomando and J. Svensson, "Transient operation of grid-connected voltage source converter under unbalanced voltage conditions," in *Conf. Rec. 36th IEEE IAS Annu. Meeting*, Sep. 2001, vol. 4, pp. 2419–2424.
[37] P. Rodriguez, A. Luna, I. Candela, R. Mujal, R. Teodorescu, and F. Blaabjerg, "Multiresonant frequency-locked loop for grid synchronization of power converters under distorted grid conditions," *IEEE Trans. Ind. Electron.*, vol. 58, no. 1, pp. 127–138, Jan. 2011.
[38] F. Rodriguez, E. Bueno, M. Aredes, L. Rolim, F. Neves, and M. Cavalcanti, "Discrete-time implementation of second order generalized integrators for grid converters," in *Proc. 34th Annu. Conf. IEEE Ind. Electron.*, Nov. 2008, pp. 176–181.
[39] A. Yazdani and R. Iravani, *Voltage-Sourced Converters in Power Systems*. Hoboken, NJ: Wiley, 2010.
[40] M. Liserre, R. Teodorescu, and F. Blaabjerg, "Stability of photovoltaic and wind turbine grid-connected inverters for a large set of grid impedance values," *IEEE Trans. Power Electron.*, vol. 21, no. 1, pp. 263–272, Jan. 2006.

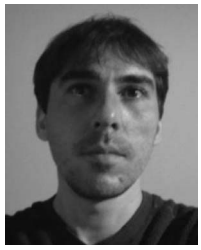

Antonio Camacho received the B.S. degree in chemical engineering and the M.S. degree in automation and industrial electronics from the Technical University of Catalonia, Barcelona, Spain, in 2000 and 2009, respectively. He is currently working toward the Ph.D. degree in electronic engineering at the Technical University of Catalonia, Vilanova i la Geltrú, Spain.

His research interests include networked and embedded control systems, industrial informatics, and power electronics.

Miguel Castilla received the B.S., M.S., and Ph.D. degrees in telecommunication engineering from the Technical University of Catalonia, Barcelona, Spain, in 1988, 1995, and 1998, respectively.

Since 2002, he has been an Associate Professor with the Department of Electronic Engineering, Technical University of Catalonia, Vilanova i la Geltrú, Spain, where he teaches courses on analog circuits and power electronics. His research interests are in the areas of power electronics, nonlinear control, and renewable-energy systems.

Jaume Miret (M'01) received the B.S. degree in telecommunications and the M.S. and Ph.D. degrees in electronics from the Technical University of Catalonia, Barcelona, Spain, in 1992, 1999, and 2005, respectively.

He is currently an Associate Professor with the Department of Electronic Engineering, Technical University of Catalonia, Vilanova i la Geltrú, Spain, where he teaches courses on digital design and circuit theory. His research interests include dc–ac converters, active power filters, and digital control.

Juan C. Vasquez received the B.S. degree in electronics engineering from the Autonomous University of Manizales, Manizales, Colombia, in 2004 and the Ph.D degree from the Department of Automatic Control Systems and Computer Engineering, Technical University of Catalonia, Barcelona, Spain, in 2009.

He was with the Autonomous University of Manizales, teaching courses on digital circuits, servo systems, and flexible manufacturing systems. He was with the Department of Automatic Control Systems and Computer Engineering, Technical University of Catalonia, where he worked as a Postdoctoral Assistant teaching courses based on renewable-energy systems. He is currently an Assistant Professor with Aalborg University, Aalborg, Denmark. His research interests include modeling, simulation, and power management applied to the distributed generation in microgrids.

Eduardo Alarcón-Gallo received the B.S. degree in telecommunications and the M.S. degree in automation and industrial electronics from the Technical University of Catalonia, Barcelona, Spain, in 2008 and 2010, respectively. He is currently working toward the Ph.D. degree in electronic engineering at the Technical University of Catalonia, Vilanova i la Geltrú, Spain.

His research interests include robotics, nonlinear control, and applications on power electronics, particularly in renewable-energy systems.